文章编号：1001-9014(2019)06-0722-06

DOI:10.11972/j.issn.1001-9014.2019.06.007

Terahertz wide stop-band metamaterials filter based on metal-dielectric-metal structure

WANG Jun-Lin, WANG Xin*, HAN Ding*

(College of Electronic Information Engineering, Inner Mongolia University, Hohhot 010021, China)

Abstract: In order to realize terahertz (THz) metamaterials (MMs) filters with multi-band or wide-band characteristics, the same or different resonance structures are usually combined in the same plane or stacked in multiple layers. THz wide stop-band MMs filter based on Metal-Dielectric-Metal (MDM) structure is presented by placing C-shaped resonance elements of the same size at both ends of the middle dielectric layer, which has the broader stop-band and the better frequency selection. Based on the analysis of the electric field and surface current distributions on the C-shaped resonance elements of the wide stop-band MMs filter, the transmission mechanism of THz wave is discussed in depth, and the filtering mechanism of the filter is revealed. The filtering characteristics of the MMs filter based on MDM structure and Metal-Dielectric (MD) structure are simulated respectively, and the formation mechanism of wide stop-band is revealed. Finally, the MMs filter samples are prepared based on PDMS thin films preparation process and magnetron sputtering, and their filtering characteristics are tested by transmission-type Terahertz Time Domain Spectroscopy (THz-TDS) TDS 1008. The correctness of design, simulation and preparation of wide stop-band MMs filter is verified, which provides reference for the design, fabrication and characteristic research of wide band filters in the future.

Key words: metamaterials, terahertz, filters, resonance, transmission

PACS: 42.79.Ci, 78.67.Pt, 81.05.-t

基于金属-介质-金属结构的太赫兹超材料宽阻带滤波器

王俊林, 王 鑫*, 韩 丁*

(内蒙古大学 电子信息工程学院,内蒙古自治区 呼和浩特 010021)

摘要:为了实现具有多频或宽频特性的太赫兹超材料滤波器,通常将相同或不同的谐振结构在同一平面内进行组合或者进行多层堆叠.通过将尺寸相同的C-型谐振单元分别置于中间介质层的两端,实现了基于金属-介质-金属结构的太赫兹超材料宽阻带滤波器,该滤波器具有较宽的阻带和较好的频率选择性.基于对该太赫兹超材料宽阻带滤波器C-型谐振结构表面的电场和电流分布的仿真分析,深入探讨了入射太赫兹波的传输机理,揭示了滤波器的滤波机制.基于对金属-介质-金属结构和金属-介质结构的超材料滤波器的滤波特性的仿真研究,揭示了宽阻带的形成机理.最后,采用PDMS薄膜制备工艺和金属磁控溅射方法对该超材料滤波器的样品进行了加工制备,并采用传输型的太赫兹时域光谱系统对其滤波特性进行了实际测试,验证了该超材料滤波器的结构设计、仿真和制备的正确性,为今后宽频带超材料滤波器的设计、制备和特性研究提供了参考.

关 键 词:超材料;太赫兹;滤波器;谐振;传输

中图分类号:TB39 **文献标识码**:A

Introduction

In recent decades, comprehensive scientific researches into Electromagnetic (EM) MMs have been developed due to their unprecedented EM phenomena that

Received date: 2019-04-16, **revised date**: 2019-11-14 **收稿日期**:2019-04-16,**修回日期**:2019-11-14

Foundation items: Supported by National Natural Science Foundation of China (51965047, 31660678), Natural Science Foundation of Inner Mongolia (2018MS06007), Higher Education Scientific Research Project of Inner Mongolia (NJZY18252), Research Startup Fund of High-level Talents Introduction in 2018 (21700-5185131), and Research Startup Fund of High-level Talents Introduction in 2018 (21700-5185128)

Biography: WANG Jun-Lin (1982-), male, Inner mongolia, China. Research area involves metamaterial and function devices, microwave and radio frequency devices, MEMS technology. E-mail: mems_wjl@163.com

* **Corresponding author**: E-mail: mems_wang@163.com, handinghanding@126.com

cannot be obtained with natural materials, including negative refraction index, cloaking behavior, backward propagation, reverse Doppler effects, and perfect absorber action. Based upon these unusual characteristics of MMs, many EM devices have been investigated with theoretical and numerical calculations, such as EM cloaking[1], antennas[2], MM absorbers[3-4], perfect lenses[5-6], thermal image[7], and filters[8-9]. It is well known that natural conventional materials cannot generate strong EM response to THz waves, and thus cannot effectively control THz waves, resulting in a serious lag in the research of THz-related functional devices. The emergence of MMs fills the gap of EM materials that can generate strong EM response in THz band, and opens up a brand-new technical route for the research and application of THz band. On the other hand, THz band is also an important frequency band of MMs research. According to statistics, nearly half of THz field is aimed at MMs in THz band. THz filter is one of the important functional components of THz communication and imaging system, and its in-depth study has far-reaching significance for the development of THz technology. In recent years, MMs have been combined with THz filters, and various THz MMs filters with different structures have been proposed, which greatly promote the development of THz filters[10-12]. The research and application of THz MMs filters with simple structure and superior performance can not only improve the performance of THz system, but also greatly promote the development of THz technology. The characteristics of MMs filters such as center frequency, bandwidth, transmission, and stop band attenuation can be adjusted by changing the geometry dimensions of the periodic metallic resonance structures. Because of the strong EM resonance behavior of MMs, the bandwidths of MMs filters are always too narrow. THz waves of different frequencies can be transmitted by stacking the same or different resonance structures on multiple layers, and then the multi-band or wide-band transmission characteristics can be generated[13-15].

In this paper, a wide stop-band MMs filter at THz frequencies is presented. The filter has a typical MDM structure, which is realized by placing C-shaped resonance elements of the same size at both ends of the middle dielectric layer. The simulation results show that the 3-dB stop-band width is 91.5 GHz, the relative stop-band bandwidth is 58%, and the rising and falling edges of the stop-band have steepness of 1.2 dB/GHz and 2.8 dB/GHz. The filter has the broader stop-band and the better frequency selection. The transmission mechanism of THz wave has been discussed in depth based on the analysis of the electric field and surface current distribution on the structure surface of MMs filter. By comparing and analyzing the filtering characteristics of MMs filter based on MDM and MD structure, the formation mechanism of wide stop-band has been revealed. The proposed MMs filter has been prepared based on PDMS thin films preparation process and magnetron sputtering and its filtering characteristics have been tested by transmission-type THz-TDS TDS 1008. The correctness of the design, simulation and preparation of the filter is verified, which will provide reference for the design and research of wide-band filter in the future. The close integration of THz technology and MMs has greatly facilitated the development of THz filters. With the rapid development of microfabrication technology, THz MMs filters have made a breakthrough. They are widely used in many fields such as THz communications, THz imaging systems, THz sensing, THz spectroscopy and many others.

1　Design and simulation

THz wide stop-band MMs filter based on MDM structure is implemented by placing the C-shaped resonance elements of the same size at both ends of the middle dielectric layer. The unit cell of the proposed MMs filter is shown in Fig. 1. We chose the Copper with electric conductivity $\sigma = 5.8 \times 10^7$S/m as metallic pattern and the PDMS with a relative permittivity of $\varepsilon_r = 2.68$ and a loss tangent of 0.02 as dielectric layer.

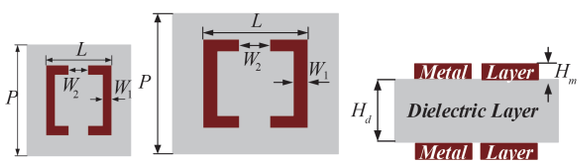

Fig. 1　Top view and side view of unit cell of THz wide stop-band MMs filter based on MDM structure
图1　基于MDM结构的太赫兹超材料宽阻带滤波器的俯视图和侧视图

Numerous simulations were performed using the frequency domain solver of CST (Computer Simulation Technology) Microwave Studio 2015 based on finite integration technique. To imitate the infinite periodic cells, the periodic boundary conditions were selected along the $x-y$ plane, while the open boundary conditions were chosen along the z plane in the simulation process. Moreover, the electric field (E) and magnetic field (H) were parallel to the incidence plane whereas the propagation wave vector (k) was perpendicular to the structure plane. The optimized geometry parameters of the unit cell are as follows: L=500 μm, W_1=60 μm, W_2=100 μm, the length of the periodic array P=700 μm, the thickness of the dielectric layer H_d=360 μm, and the thickness of the top and bottom metal structure H_m=0.3 μm.

The simulated transmission curves of the proposed THz wide stop-band filter based on MDM structure for the normal incidence EM waves are illustrated in Fig. 2. Figure 2 (a) shows the transmission curve in dB unit and Fig. 2 (b) shows the transmission curve in ordinate with percentage transmission rate.

As can be seen from Fig. 2 (a), when the THz wave is incident normally on the structure surface of the MMs filter, two resonance peaks are generated at 151.1 GHz and 189.7 GHz. The corresponding S_{21} parameters are -54.9 dB and -48.1 dB, respectively. The 3-dB stop-band width is 91.5 GHz (from 112.8 GHz to 204.3

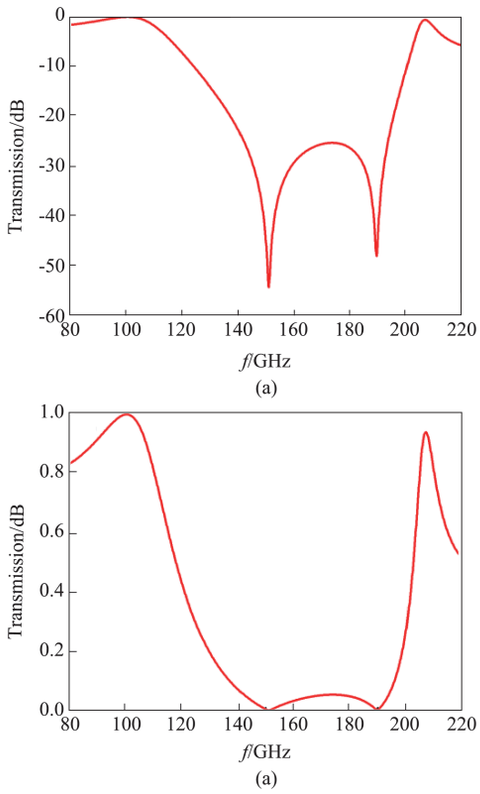

Fig.2 (a) Transmission curve of THz wide stop-band MMs filter with dB as ordinate, and (b) Transmission curve of THz wide stop-band MMs filter in ordinate with transmission rate as ordinate

图2 (a)以dB为纵坐标的太赫兹超材料宽阻带滤波器的传输曲线,(b)以传输率为纵坐标的太赫兹超材料宽阻带滤波器的传输曲线

GHz), and the stop-band center frequency is 158.6 GHz. The S_{21} parameter at the center frequency is -30.6 dB, and the relative stop-band bandwidth is 58 %. The steepness of the rising and falling edges of the stop-band is 1.2 dB/GHz and 2.8 dB/GHz, respectively. The S_{21} parameters at 90 GHz, 110 GHz, 210 GHz and 215 GHz in passband are -1.8 dB, -1.5 dB, -1.2 dB and -4.5 dB, respectively.

As shown in Fig. 2 (b), the half-wave stop-band bandwidth of the MMs filter is 84.5 GHz (from 118.1 GHz to 202.6 GHz) and the relative half frequency stop-band bandwidth is 53.3 %. Considering the dielectric loss, the transmission corresponding to a specific frequency of 100.3 GHz in passband does reach 100 %, while the transmission at other frequencies is less than 100 %, such as the transmission at 90 GHz, 110 GHz, 210 GHz and 215 GHz in passband are 87 %, 85 %, 96 % and 65 %, respectively. From a series of characteristics given above, it can be seen that the MMs filter with C-shaped resonance elements based on MDM structure does has the wider stop-band and the better frequency selectivity.

2 Analysis and Discussion

In order to investigate the filtering mechanism of THz wide stop-band filter based on MDM structure, the electric field and surface current distribution of the top and bottom C-shaped resonance elements at the center frequency were simulated, as shown in Figs. 3-4.

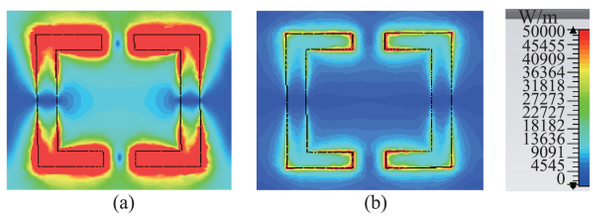

Fig.3 (a) The surface electric field distribution on the top C-shaped resonance element at the center frequency, and (b) the surface electric field distribution on the bottom C-shaped resonance element at the center frequency

图3 (a)中心频率处顶层C-型谐振单元的表面电场分布,(b)中心频率处底层C-型谐振单元的表面电场分布

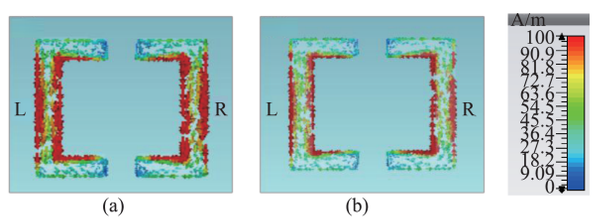

Fig.4 (a) The surface current distribution on the top C-shaped resonance element at the center frequency, and (b) the surface current distribution on the bottom C-shaped resonance element at the center frequency

图4 (a)中心频率处顶层C-型谐振结构的表面电流分布,(b)中心频率处底层C-型谐振结构的表面电流分布

It can be clearly seen from the Fig. 3 that the surface electric field distributions of the top and bottom C-shaped resonance element at the center frequency of 158.6 GHz are basically the same, and the strong electric field is mainly distributed on the inner and outer edges of the C-shaped resonance element. It is well known that the strong electric field distribution corresponds to the strong electric resonance, reflecting the strong electric coupling between the resonance elements and inside the resonance elements. In addition, comparing Fig. 3 (a-b), although the electric field distribution of resonance elements in different metal layers is basically the same, the electric field intensity decreases rapidly from the top to the bottom.

Figures 4 (a-b) show the surface current distributions of the top and bottom metal resonance elements. As can be clearly seen the large current mainly distributes symmetrically along the left and right arms of the C-shaped resonance element at the center frequency of 158.6 GHz. It can be found that there are anti-symmetrical surface current distributions between the top and bottom metal layers, and the current intensity decreases rapidly from the top layer to the bottom by comparing Figs. 4 (a-b). The anti-symmetrical surface current between the top and bottom metal layers can be equivalent to a ring current, forming an inductive magnetic field and forming a magnetic resonance with the incident EM field.

At the center frequency of the stop-band, the elec-

tric field and surface current distributions of the MMs filter based on MDM structure decrease rapidly along the propagation direction of THz wave. In other word, in the stop-band range, almost all the incident THz waves are reflected, thereby forming a strong attenuation in the stop-band.

In addition, it is noteworthy that the MMs filter based on multi-layer metal resonance structures has longitudinal coupling between different layers in the propagation direction of incident EM waves[16-17]. As shown in Fig. 5, when the thickness of the dielectric layer increases (decreases), the longitudinal coupling will decrease (increase), resulting in the offset of two resonance peaks, which will lead to the change of stopband bandwidth and the shift of center frequency.

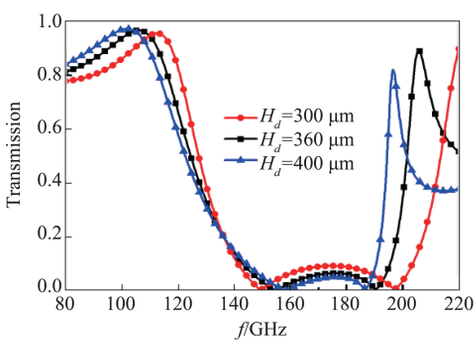

Fig. 5　Relation curves between dielectric layer thickness and filtering characteristics of THz MMs filter based on MDM structure
图5　基于MDM结构的太赫兹超材料滤波器介质层厚度和滤波特性之间的对应关系曲线

In order to deeply study the formation mechanism of wide stop-band of MMs filter based on MDM structure, the simulation transmission curves of MMs filter based on MDM structure and MD structure were compared and analyzed. The MMs filter based on MD structure can be formed by removing the bottom layer of metal resonance structure of MMs filter based on MDM structure and keeping all structural parameters unchanged.

As shown in Fig. 6, when the THz wave is incident normally from the end of the C-shaped resonance elements to the surface of the MMs filter based on MD structure, a resonance peak is generated at 170.35 GHz, resulting in a narrow stop-band bandwidth. For the MMs filter based on MDM structure, the resonance frequencies of two resonance peaks are f_L=150.85 GHz and f_H=190.7 GHz respectively. Because the two resonance peaks are close to each other, the wide stop-band MMs filter is formed.

In summary, the MMs filter based on multi-layer metal resonance structure arrays will produce multi-resonance response, and then form multi-resonance peaks. If the multi-resonance peaks are close to each other, it will form a wider bandwidth filter. It is worth noting that these multi-resonance peaks are mainly generated by the longitudinal coupling between different metal layers along the direction of EM waves propagation.

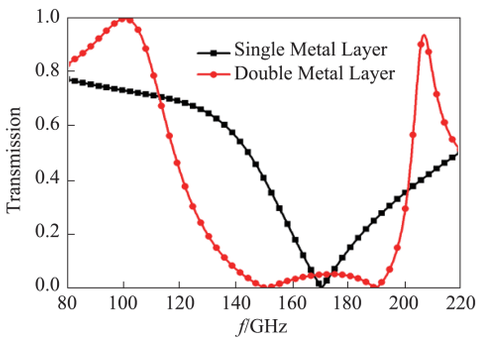

Fig. 6　Transmission curves of THz MMs filter based on MD structure and MDM structure
图6　基于MDM结构和MD结构的太赫兹超材料滤波器的传输特性曲线

3　Manufacturing and Test

In order to confirm the correctness of the simulated transmission performance of the MMs filter, prototype samples based on optimized physical dimensions have been prepared using surface micromachining processes. The mask map drawn by AutoCAD software and the physical map of mask are shown in the Fig. 7.

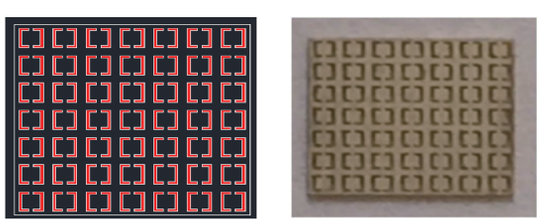

(a) The mask map drawn by AutoCAD　(b) The physical map of mask

Fig.7　(a) The mask map drawn by AutoCAD, (b) The physical map of mask
图7　(a) Auto CAD绘制的掩膜板图, (b) 掩膜板实物图

The manufacturing steps of the THz stop-band MMs filter based on MDM structure are as follows:

(1) Preparation of PDMS mixture

By setting different ratio of curing agent to prepolymer, PDMS films with different Young's modulus can be obtained. The Young's modulus of PDMS solution increases with the decrease of the ratio of curing agent to prepolymer. The larger the Young's modulus, the smaller the elasticity of the cured colloid and the easier it is to tear when peeling off. On the contrary, the lower the Young's modulus, the better the elasticity of the cured colloid and the less easily it is to tear when peeling off. The ratio of PDMS curing agent to prepolymer is generally set at 1:5, 1:10, 1:15 or 1:20. After a large number of experiments, the characteristics of the films were studied in depth. It is found that when the ratio of curing agent to prepolymer is 1:10, the elasticity of PDMS films is the best and it is easier to peel off from silicon wafers.

Firstly, the beaker and the stirring glass rod were cleaned and blown dry with deionized water. Then the curing agent and the prepolymer were absorbed 5 g and 0.5 g respectively with a syringe at the ratio of 10:1.

The prepolymer and the curing agent were then injected into the beaker and stirred slowly in the same direction with the glass rod to make the prepolymer and the curing agent solid.

Secondly, the fully mixed PDMS mixture was placed in the vacuum drying box, and the pumping state was maintained until the bubbles of the mixture were discharged. The whole vacuum pumping process lasted about 30 minutes. In the process of vacuum pumping, the pumping range should not be too large to prevent the overflow of PDMS mixture in beaker.

(2)Preparation of PDMS thin films

PDMS thin films were prepared by spin coating method. In general, the PDMS mixture was uniformly coated on the silicon wafer substrate by centrifugal force generated during the operation of the coater. The PDMS was cured by heating, and then removed from the substrate to obtain the PDMS thin films.

Firstly, the 2-inch silicon wafer was cleaned with acetone, alcohol and deionized water, and then was blown dry with nitrogen. Then, the mass of the desired PDMS mixture was calculated according to the thickness of the PDMS film to be prepared and the area of the silicon wafer. The corresponding quality of the PDMS mixture was poured onto the silicon substrate. The position of the silicon wafer was continuously adjusted so that the PDMS mixture completely covers the surface of the silicon wafer. Finally, the silicon wafer with PDMS film was placed on a horizontal baking table to be heated and cured. The baking table temperature was set at 75 ℃ for 3 hours. After the temperature drops to room temperature, the wafer was removed.

(3)Stripping of PDMS thin films

The cured PDMS film was slowly removed from the silicon substrate by tweezers, and then dried by deionized water and nitrogen.

(4) Metal structure formed by magnetron sputtering

Because PDMS is a hydrophobic material, hydrophilic modification is firstly needed to improve the adhesion between the sputtered metal layer and PDMS film. Then a suitable position was selected on the PDMS film, and the fabricated mask was placed on the surface of the PDMS film. And then the mask was placed on the tray of the magnetron sputtering machine, and the sputtering power and time were set up to complete the sputtering of 0.3 μm thick top metal structure. Because the PDMS film is transparent, the coincidence between the mask and the underlying metal structure can be observed under the confocal microscope. By adjusting the position of the mask to ensure that the mask was in strict alignment with the underlying metal structure, the sample was slowly placed on the tray of the magnetron sputtering machine, and the same sputtering power and time were set to complete the sputtering of 0.3 μm thick underlying metal structure.

Based on the above preparation steps, the sample preparation of THz wide stop-band MMs filter with a size of 4.9 mm × 4.9 mm and a total of 7 × 7 metal resonance elements can be completed. Confocal microscopy was used to observe the morphology of samples. The morphology of MMs filter sample is shown in Fig. 8.

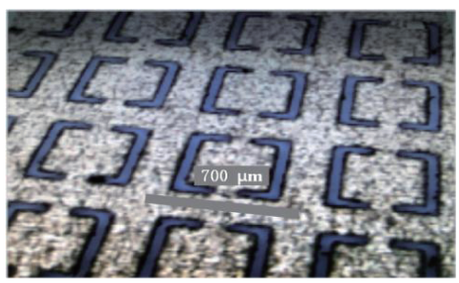

Fig. 8 The morphology of the MMs filter sample observed under confocal microscope
图8 共聚焦显微镜下观测到的超材料滤波器样品形态

Fig. 9 Internal optical path map of transmission-type THz-TDS TDS 1008
图9 传输型太赫兹时域光谱系统TDS1008的内部光路图

As shown in Fig. 9, after the preparation of THz wide stop-band MMs filter samples based on the MDM structure was completed, the transmission parameters of the filter sample were measured by transmission-type THz-TDS TDS 1008. THz-TDS can be divided into transmission and reflection modes depending on the detection light paths, which are used to measure the transmission and reflection spectra of THz waves.

In order to prevent water vapor in the environment from interfering with the test results, the optical path of THz-TDS is placed in a sealed box filled with dry nitrogen gas to ensure absolute drying of the optical path system and to eliminate the interference of external factors such as environment. After that, the time-domain signals without and with MMs filter were measured at room temperature. Then the time-domain signals were converted into corresponding frequency-domain signals by fast Fourier transform. Finally, the spectrum response curves of the samples to be measured can be obtained.

The test performance of the MMs filter is shown in the red curve in Fig. 10. The stop-band center frequency is 161.92 GHz, the half-wave stop-band bandwidth is 66.53 GHz, and the relative half-wave stop-band bandwidth is 41 %. The test and simulation results are not completely consistent, and there are some deviations. The above deviations mainly come from the processing errors introduced in the sample preparation process, such as the size deviation of the resonance unit, the thickness

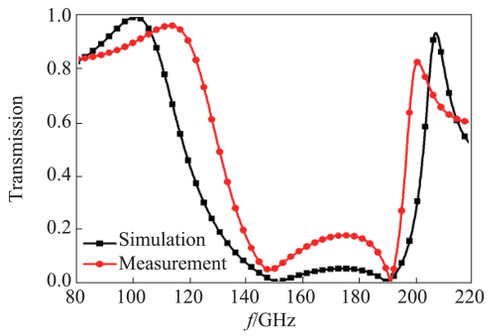

Fig. 10　Comparison between the simulated and measured transmission performance
图 10　仿真和测试特性的对比

deviation of the metal film and the alignment deviation of the top and bottom metal resonance structures.

4　Conclusions

THz wide stop-band MMs filter is mainly used to achieve high precision and wide band frequency operation in THz frequency band. However, the narrow operating band of MMs stop-band filter has become the biggest obstacle to its practical application, therefore, the design and implementation of THz wide stop-band MMs filter is of practical significance.

In this paper, a THz wide stop-band MMs filter based on MDM structure was implemented by placing the C-shaped resonance elements of same size at both ends of the middle dielectric layer. Based on the CST EM simulation software, the filtering mechanism and the formation of wide stop-band were studied in depth. Based on the optimized filter structure parameters, wide stop-band MMs filter samples were prepared by PDMS thin film preparation process and metal magnetron sputtering method, and the filtering characteristics were tested. The test results were basically matched with the simulation results. The correctness of the structure design, simulation and preparation of the wide stop-band MMs filter was verified. In this design, the periodic metallic resonance structures were patterned on the flexible PDMS substrate, so it can be conformed to the unusual surfaces such as cylindrical, pyramid, spherical and so on.

The design idea and preparation method of the wide stop-band MMs filter provide a reference for the design and fabrication of the wideband MMs filter. In the future, the number of metal and dielectric layers can be added to the structure to obtain broader band filter structure, and the structure of the metal resonance unit can be changed.

References

[1] Schurig D, Mock J J, Justice B J, *et al*. Metamaterial electromagnetic cloak at microwave frequencies[J]. *Science*, 2006, **314**(5801): 977-980.
[2] Yoo M, Lim S. SRR- and CSRR-loaded ultra-wideband (UWB) antenna with tri-band notch capability[J]. *Journal of Electromagnetic Waves and Applications*, 2013, **27**(7): 2190-2197.
[3] Wang X, Zhang B Z, Wang W J, *et al*. Design and characterization of an ultra-broadband metamaterial microwave absorber[J]. *IEEE Photonics Journal*, 2017, **9**(3): 4600213.
[4] Wang X, Zhang B Z, Wang W J, *et al*. design, fabrication, and characterization of a flexible dual-band metamaterial absorber[J]. *IEEE Photonics Journal*, 2017, **9**(4): 4600512.
[5] Ramm A G. Does negative refraction make a perfect lens[J]. *Physics Letters A*, 2008, **372**(43): 6518-6520.
[6] Amireddy K K, Balasubramaniam K, Rajagopal P. Holey-structured metamaterial lens for subwavelength resolution in ultrasonic characterization of metallic components[J]. *Applied Physics Letters*, 2016, **108**(22): 5-13.
[7] Jung J Y, Lee J, Choi D G, *et al*. Wavelength-selective infrared metasurface absorber for multispectral thermal detection[J]. *IEEE Photonics Journal*, 2015, **7**(6): 1-10.
[8] Li Z, Ding Y J. Terahertz broadband-stop filters[J]. *IEEE Journal of Selected Topics In Quantum Electronics*, 2013, **19**(1): 8500705.
[9] Zhang X, Gu J, Cao W, *et al*. Bilayer-fish-scale ultrabroad terahertz bandpass filter[J]. *Optics Letters*, 2012, **37**(5): 906-908.
[10] Wang J L, Zhang B Z, Wang X, *et al*. Flexible dual-band band-stop metamaterials filter for the terahertz region[J]. *Opt. Mater. Express*, 2017, **7**(5): 1656-1665.
[11] Wei Z C, Li X P, Yin J J, *et al*. Active plasmonic band-stop filters based on grapheme metamaterial at THz wavelengths[J]. Optics Express, 2016, **24**(13): 14344-14351.
[12] Ebrahimi A, Nirantar S, Withayachumnankul W, *et al*. Second-order terahertz bandpass frequency selective surface with miniaturized elements[J]. *IEEE Transactions on Terahertz Science and Technology*, 2015, **5**(5): 761-769.
[13] Liang L J, Yao J Q, Yan X. Ultrabroad terahertz bandpass filter based on a multiple-layered metamaterial with flexible substrates[J]. *Chin. phys. lett*, 2012, **29**(9): 94209-94211(3).
[14] Lan F, Yang Z, Qi L, *et al*. Terahertz dual-resonance bandpass filter using bilayer reformative complementary metamaterial structures [J]. *Optics Letters*, 2014, **39**(7): 1709-1712.
[15] Li C. multi-band terahertz filter with independence to polarization and insensitivity to incidence angles[J]. *Journal of Infrared Millimeter & Terahertz Waves*, 2015, **36**(11): 1137-1144.
[16] Zhao X G, Fan K B, Zhang J D, *et al*. Voltage-tunable dual-layer terahertz metamaterials[J]. *Microsystems & Nanoengineering*, 2016, **2**: 16025.
[17] Marqués R, Mesa F, Martel J, *et al*. Comparative analysis of edge- and broadside-coupled split ring resonators for metamaterial design-theory and experiments[J]. *IEEE Transactions on Antennas and Propagation*, 2003, **51**(10): 2572 - 2581.